communications chemistry

Article

https://doi.org/10.1038/s42004-024-01250-y

Design principles, growth laws, and competition of minimal autocatalysts

Yann Sakref & Olivier Rivoire ✉

The difficulty of designing simple autocatalysts that grow exponentially in the absence of enzymes, external drives or ingenious internal mechanisms severely constrains scenarios for the emergence of evolution by natural selection in chemical and physical systems. Here, we systematically analyze these difficulties in the simplest and most generic autocatalyst: a dimeric molecule that duplicates by templated ligation. We show that despite its simplicity, such an autocatalyst can achieve exponential growth autonomously. We also show, however, that it is possible to design as simple sub-exponential autocatalysts that have an advantage over exponential autocatalysts when competing for a common resource. We reach these conclusions by developing a theoretical framework based on kinetic barrier diagrams. Besides challenging commonly accepted assumptions in the field of the origin of life, our results provide a blueprint for the experimental realization of elementary autocatalysts exhibiting a form of natural selection, whether on a molecular or colloidal scale.

The path from simple chemical systems to complex living organisms is believed to hinge on a pivotal point at which one molecule, or a set of molecules, gains the capability to catalyze their own formation, hence constituting an autocatalytic system[1–5]. When several such systems are formed from a common molecule, the faster ones hinder the growth of the slower ones, and may even exclude them if the common molecule is limiting. This elementary form of natural selection is thought to set the stage for Darwinian evolution[1–3]. Mathematically, exclusion occurs whenever replicators grow exponentially using a common limiting resource, in which case only the fastest-growing replicator can survive[6–8].

Molecular replication in extant living organisms relies on enzymatic catalysis and involves a large network of coupled reactions. Non-enzymatic autocatalysts have been designed in a variety of artificial systems and at a variety of scales, from the molecular and colloidal scale up to the macroscopic scale[9–18]. At the molecular scale, the simplest systems implement template replication, where the formation of a new complex AB from its constituents A and B is catalyzed by a previously formed complex AB. However, such non-enzymatic molecular autocatalysts are generally found to exhibit sub-exponential growth, where the number x of autocatalysts follows the phenomenological equation $dx/dt = kx^n$ with $n < 1$, associated with polynomial growth[5,19], $x(t) \sim t^{1/(1-n)}$. A growth order of $n \approx 1/2$ is typically observed[5,9,19,20], also known as parabolic growth due to the relationship $x(t) \sim t^2$. Sub-exponential autocatalysts, unlike exponential autocatalysts, are not mutually exclusive, which often leads them to be considered as representing only a basic and limited type of selection-if they are taken into account at all in the emergence of natural selection[7,16,19,21]. This limitation has spurred research into identifying the physical basis of sub-exponential growth and defining the requirements autocatalysts must meet to achieve exponential growth.

In 1993, von Kiedrowski demonstrated, through the analysis of a minimal model of autocatalysis, that sub-exponential growth originates from product inhibition, the propensity of autocatalytic templates to inhibit their catalytic activity by binding to each other[19]. He established thermodynamic and species concentration conditions under which product inhibition is negligible, that is, under which exponential growth can occur. However, his analysis was based on several assumptions: a local equilibrium between substrates and templates, a local equilibrium between free and complexed templates, and a substrate concentration well in excess of the total autocatalyst concentration. This left open the question of what may happen beyond these local equilibria, and beyond the initial stages of the reaction.

In the meantime, much experimental efforts has gone into designing autocatalysts that mitigate product inhibition. The first type of solutions involves external drives applied in a cyclical pattern, such as heat[18,22,23], mechanical stress[24], light[25,26], tidal cycling[27], or magnetic fields[28]. Approaches based on the intrinsic properties of the autocatalyst rather than external factors have also been proposed[25,29–36]. For instance, at the molecular level, the affinity between autocatalysts can be diminished by coupling the formation of a bound within autocatalysts to the breaking of a bound between autocatalysts[33,34], or by entropic mechanisms like toeholds and handholds strand displacements when using nucleic acids[25,35,36]. These approaches, although effective in specific settings, raise several questions. First, it is often ambiguous whether the proposed mechanism mitigates product inhibition, the binding of two preformed autocatalysts, or accelerates product release,

Gulliver, CNRS, ESPCI, Université PSL, Paris, France. ✉e-mail: olivier.rivoire@espci.fr

the unbinding of a newly formed autocatalyst from a preformed catalyst, which is known to impact the growth rate but not the growth order of autocatalysis[25,32,35,37]. Second, these mechanisms are often idiosyncratic to the context in which they are designed, which limits the scope of their applicability. Finally, and perhaps most importantly, the designs are generally intricate and fine-tuned, which defeats the purpose of studying autocatalysis as a means to understand the accretion of complexity.

This poses a major problem for origin-of-life scenarios based on autocatalysis. Consequently, most scenarios currently focus on autocatalytic networks composed of multiple molecules rather than single-molecule autocatalysts[38–44]. This orientation reflects the belief that these networks are more likely to emerge spontaneously[2,45–50]. However, networks raise similar challenges[20,51], as well as posing new ones, e.g., the likely appearance of parasites[52,53].

In either case, whether based on a single species or a network of species, the design of autocatalysts has so far mainly remained in the realm of empirical studies. In particular, no theoretical work has, to our knowledge, examined the minimum requirements autocatalysts must meet to achieve exponential growth beyond the assumptions made by von Kiedrowski[19]. Here, we propose to fill this gap by showing through a systematic approach that simple and generic exponential autocatalysts are designable, although with limitations that we clarify. By simple, we mean autocatalysts composed of very few elements (two) with no internal structure or internal degree of freedom[54]. By generic, we mean an entropic mechanism of autocatalysis by proximity that is present in any chemistry or colloidal system subject to thermal noise.

Our starting point is a physical model of interacting particles, from which we derive a kinetic model described by a Markov chain. This choice ensures that our parameterization of kinetic rates captures the fundamental physical trade-offs inherent in autocatalytic systems. It also helps us to identify the actual range of parameters in which such an autocatalyst could be experimentally implemented. Our approach is to treat autocatalysis as a special case of catalysis—namely when the product is a catalyst—and to apply a previously developed methodology to define, construct, and optimize minimal catalysts[55,56]. However, this is only a starting point: as we show, this methodology needs to be extended to account for the constraints arising from the identity between products and catalysts, which introduces a fundamental distinction between catalysis and autocatalysis. As a result, we demonstrate that it is possible to design simple generic autocatalysts that grow exponentially, but that it is equally possible to design simple sub-exponential autocatalysts that out-compete them in conditions of resource limitation.

Methodology

Model. We study the design of autocatalysts AB composed of two units A and B which catalyze their own formation through a templating reaction summarized by $AB + A + B \rightarrow 2AB$ (Fig. 1A). Guided by simplicity, we consider for A and B spherical particles of same diameter σ, immersed in a thermal bath at temperature T within a two-dimensional box of dimension $L \times L$. For illustration and to indicate the experimental feasibility of our design, we take inspiration from DNA-coated colloids[57] and present numerical results using a short-range, pairwise potential with a reverse barrier (see Methods). As represented in Fig. 1B, this potential features a cutoff distance of $r_c = 1.1\sigma$, and a minimum at $r_{\min} = 1.03\,\sigma$ [58,59]. Thus, only two parameters are left to specify the interaction between two particles of types X and Y: the energy barrier for dimer association, ϵ^+_{XY} and the energy barrier for dimer dissociation ϵ^-_{XY}.

With two particle types, A and B, we generally need six parameters to specify the interaction potentials. We reduce this number to two by making additional simplifying assumptions. First, we consider that the dimerization reaction, $A + B \rightarrow AB$, is irreversible ($\epsilon^-_{AB} = \infty$), and that the interaction between A and B is therefore described by a single parameter ϵ^+_{AB}, the association barrier. Second, we consider that the interaction potentials between two A or two B are the same, with the same depth ($\epsilon^-_{AA} = \epsilon^-_{BB}$) and no association barrier ($\epsilon^+_{AA} = \epsilon^+_{BB} = 0$), leaving a single parameter ϵ^-_{AA}, the interaction strength, to describe their interaction. Also to simplify the analysis, we assume that no molecule of size larger than four can be formed. As summarized in Fig. 1C, the model has a total of three dimensionless parameters: L/σ, ϵ^+_{AB}/k_BT and ϵ^-_{AA}/k_BT where k_B is the Boltzmann constant. Without loss of generality, we set $\sigma = 1$ to define the length scale, and $k_BT = 1$ to define the energy scale. To these three physical parameters, we must add the current concentrations of molecular species. Again for simplicity, we assume that A and B have the same concentration $[A] = [B]$. The only remaining parameter is then $[AB]$, the concentration of free products, or $[AB]_{\text{tot}}$, the total concentration of products, including those in complex with other species.

Questions. In the context of this model, the questions raised in the introduction can be formulated as follows: What are the physical parameters L, ϵ^+_{AB}, ϵ^-_{AA} and the chemical conditions $[A]$ and $[AB]$ for (i) optimal autocatalysis, that is, leading to a maximal acceleration of the dimerization reaction $A + B \rightarrow AB$ by a pre-existing AB? (ii) exponential growth, $d[AB]_{\text{tot}}/dt = k[AB]_{\text{tot}}$? (iii) exclusion of an alternative autocatalyst AD sharing with AB a common constituent A?

Approach. As an intermediate step towards the design of an autocatalyst AB, we first consider a dimeric catalyst $C = A'B'$, which is distinguishable from AB, but has identical physical properties ($\epsilon^+_{A'B'} = \epsilon^+_{AB}$ and $\epsilon^-_{A'A'} = \epsilon^-_{B'B'} = \epsilon^-_{AA}$). Studying catalysis $C + A + B \rightarrow C + AB$ enables us to apply and extend the methods previously developed to design a minimal catalyst for the reverse reaction, the dissociation of AB into $A + B$[55], and provides a basis for subsequently exposing the nuances between catalysis and autocatalysis.

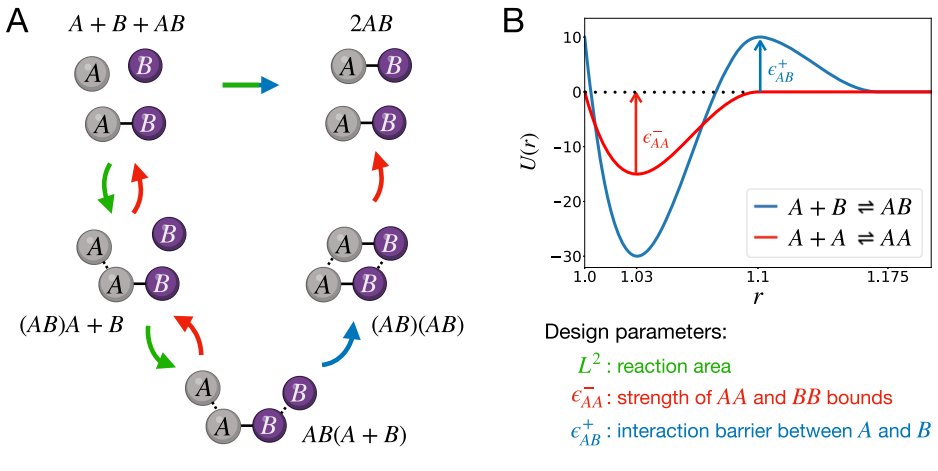

Fig. 1 | Model for the design of minimal autocatalysts. A Autocatalytic cycle in which particles A and B can attach to dimer AB catalyzing their dimerization. The scheme represents A binding AB before B but the reverse order is also possible. Green arrows indicate diffusion processes, dependent on the area L^2. Red arrows represent dissociations of two identical particles, dependent on the interaction strength ϵ^-_{AA}. Blue arrows represent the association between distinct particles, dependent on the interaction barrier ϵ^+_{AB}. The spontaneous reaction involves both diffusion and association and is indicated by a two-colored arrow. **B** Potentials by which particles interact (Materials and methods). Between identical particles, the potential depth is ϵ^-_{AA}, and association is diffusion-limited. Between distinct particles, the potential depth is very large (infinite), and association is limited by a barrier ϵ^+_{AB}.

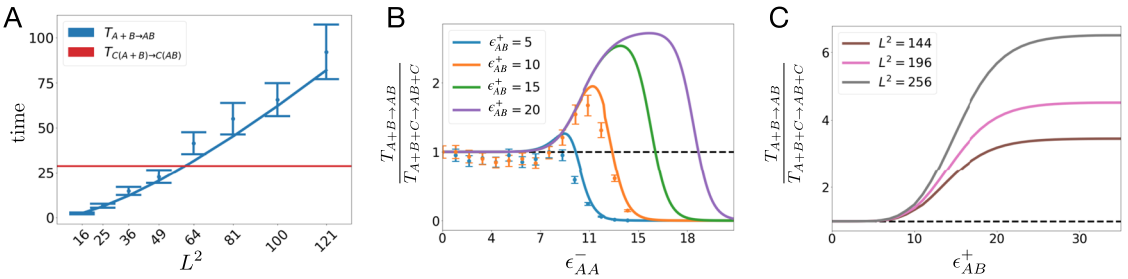

Fig. 2 | Conditions for catalysis of the dimerization $A+B\to AB$. **A** Mean times for the dimerization $A+B\to AB$ in the absence of $C=A'B'$ (in blue) and for the dimerization $C(A+B)\to C(AB)$ when A, B are kept attached to C (in red). A necessary condition for catalysis is $T_{A+B\to AB} > T_{C(A+B)\to C(AB)}$[56]. Since the first time scales with the reaction area L^2 while the second is independent of it, catalysis requires a sufficiently large value of L^2. The lines are from the Markov model presented in the text and the bars are from MD. **B** The catalytic efficiency of C shows a maximum at an intermediary value of the interaction strength ϵ^-_{AA}, consistent with the Sabatier principle. The value of this maximum increases with the interaction barrier ϵ^+_{AB}. **C** The catalytic efficiency for optimal ϵ^-_{AA} increases both with the reaction barrier ϵ^+_{AB} and with the reaction area L^2.

More precisely, we derive constraints on the design of minimal autocatalysts in four steps, starting from standard catalysis in the simplest setting and progressively introducing elements of feedback inherent to autocatalysis: (1) We determine the conditions under which a dimer $C=A'B'$ can accelerate the dimerization reaction $A+B\to AB$. This is done by comparing the time for the spontaneous formation of a dimer AB in the presence and in the absence of a C[56]. (2) Next, given a catalyst $C=A'B'$, we determine the conditions for its optimal efficiency. This is done by minimizing the cycling time $T^0_{\rm cycle}$, defined as the mean time taken by one $C=A'B'$ to turn a substrate $A+B$ into a product AB.

Following previous work[55], we solve (1) and (2) in conditions that are most favorable for catalysis, namely in the absence of any product AB[56]. (3) One unique feature of autocatalysis, however, is that it necessarily takes place in the presence of products, since the catalyst is itself a product. Products generally cause product inhibition, whereby a product binds a catalyst and inhibits its activity. We first analyze the consequence of product inhibition in standard catalysis, when the catalyst $C=A'B'$ differs from the product AB, and show that it increases the mean cycling time to $T_{\rm cycle}=T^0_{\rm cycle}+T_{\rm inhib}$ with an additional time $T_{\rm inhib}$ that depends on the concentration $[AB]$ of products. (4) Finally, we apply the previous results to $C=AB$ and highlight how autocatalysis departs from catalysis. In particular, while for standard catalysis the rate of product formation is, when assuming the spontaneous reaction to be negligible, proportional to the concentration of catalysts, i.e., of the form $d[AB]_{\rm tot}/dt=k[C]$ with $k=1/T_{\rm cycle}$, this is no longer the case for autocatalysis because $T_{\rm cycle}$ depends on $[AB]$ with $AB=C$.

Results

Design principles for minimal (auto)catalysts

Conditions for catalysis. To determine the conditions under which a dimer $C=A'B'$ can cause the acceleration of the reaction $A+B\to AB$, we first consider a closed system with only one particle A and one particle B and determine the mean time $T_{A+B\to AB}$ for a dimer AB to form[55]. We compare this time to $T_{C+A+B\to C+AB}$, the mean time for AB to form when a prospective catalyst C is added. Catalysis occurs when this later time is shorter than the former, that is, when the relative catalytic efficiency defined by the ratio $T_{A+B\to AB}/T_{C+A+B\to C+AB}$ is superior to 1. In previous work, we showed that a molecule acts as an (auto)catalyst in the presence of multiple molecules A and B only if it acts as one in the presence of a single A and a single B[56].

The first necessary condition is for the dimerization onto the catalyst to be faster than the spontaneous reaction in the bulk, i.e., $T_{C(A+B)\to C(AB)} < T_{A+B\to AB}$[56]. As expected from the Arrhenius equation, we verify with molecular dynamics (MD) simulations that both these times scale exponentially with the association barrier ϵ^+_{AB} when it is sufficiently large (Fig. S1): $T_{A+B\to AB}\approx L^2 e^{\epsilon^+_{AB}}$ and $T_{C(A+B)\to CAB}\approx e^{\epsilon^+_{AB}}$. Catalysis therefore requires a minimal area L^2. For the design at hand, we find that an area of $(L/\sigma)^2 \gtrsim 50$ is necessary (Fig. 2A).

Assuming such sufficiently large area L^2, we next study the impact of the two physical parameters, ϵ^+_{AB} and ϵ^-_{AA}. To extend this study beyond the range of parameter values accessible by MD, we approximate the dynamics by a Markov model with five distinct states, corresponding to the various states of bonding between the autocatalyst, the monomers A and B, and the product AB (Fig. 1A). Formally, the catalytic cycle is described by

$$C+A+B \underset{k_{-1}}{\overset{k_1}{\rightleftharpoons}} CA+B \underset{k_{-2}}{\overset{k_2}{\rightleftharpoons}} C(A+B) \overset{k_3}{\to} C(AB) \overset{k_4}{\to} C+AB, \qquad (1)$$

closed by adding $C+A+B \underset{k_{-0}}{\overset{k_0}{\rightleftharpoons}} C+AB$ to represent the spontaneous reaction without any interaction with the catalyst. Here we assume that A and B are equivalent and we therefore do not differentiate between $CA+B$ and $CB+A$. We also assume that release occurs in a single step, which is a good approximation when ϵ^-_{AA} is sufficiently large (Fig. S2). We take the dependence of the rate on the parameters to be given by

$$k_1 \approx 2L^{-2}, \quad k_2 \approx L^{-2}, \quad k_3 \approx e^{-\epsilon^+_{AB}}, \quad k_4 \approx e^{-2\epsilon^-_{AA}},$$
$$k_{-1} \approx e^{-\epsilon^-_{AA}}, \quad k_{-2} \approx 2e^{-\epsilon^-_{AA}}. \qquad (2)$$

Pre-factors can be introduced to obtain a better fit for the MD simulations (Supplementary Material and Fig. S3), but they have no major impact on the results (Fig. S8) and are omitted here to simplify the presentation. The main purpose of this physical parameterization is indeed not to accurately describe a particular system, but to capture the generic relationships between kinetic rates.

The catalytic efficiency depends both on the interaction strength ϵ^-_{AA} and on the association barrier ϵ^+_{AB}. For a given association barrier ϵ^+_{AB}, we observe an optimal interaction strength ϵ^-_{AA} (Fig. 2B). This observation follows Sabatier's principle, which applies broadly to catalytic systems with no internal degrees of freedom[60,61], and states that an optimal interaction between a catalyst and its substrate must strike a balance between too weak an interaction that cannot hold the substrates until they react, and too strong an interaction that cannot release the product rapidly.

A second observation is that larger association barriers ϵ^+_{AB} enable greater relative catalytic efficiencies $T_{A+B\to AB}/T_{C+A+B\to C+AB}$ (Fig. 2B) This is again a generic feature: the larger the barrier for the spontaneous reaction, the more potential for catalysis. In fact no catalysis can occur if the barrier is too small[55]. Finally, increasing the reaction area also increases the relative efficiency of the catalyst (Fig. 2C). This is simply the consequence of increasing the mean time of the spontaneous dimerization reaction in solution without changing the dimerization reaction on the catalyst.

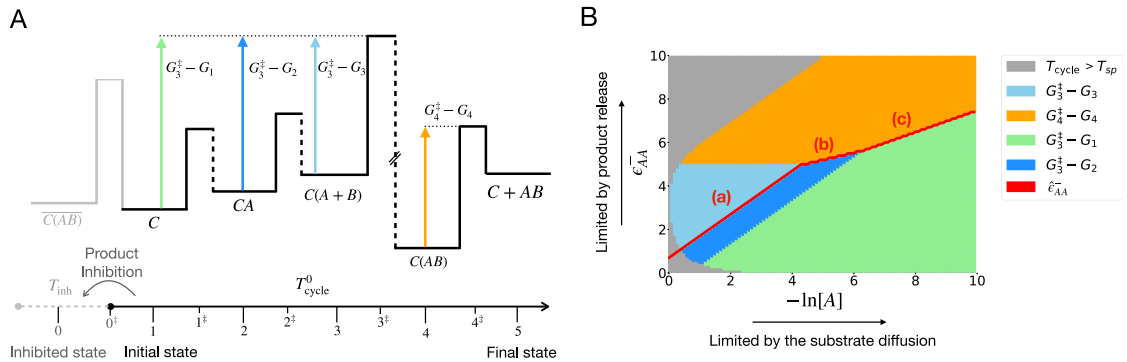

Fig. 3 | Kinetic energy diagram and limiting barriers. A Kinetic energy diagram associated with the Markov chain described by Eq. (1) and Eq. (8). Local minima represent states while local maxima represent transition states, at levels corresponding to the rates between successive states, as given by Eq. (3). The mean cycling time is approximated by the largest difference between successive levels, as indicated in Eq. (5). In this illustration, it is given by $G_3^\ddagger - G_1$ (light green) but other values of the parameters can lead to other limiting barriers. As in Fig. 1, different colors refer to different processes: light blue for dimerization, darker blue for association of a substrate followed by dimerization, green for diffusion of both substrates followed by dimerization, and orange for the dissociation of the product. Backward direct barriers are indicated with dashed lines. In the presence of products, an additional state $i = 0$ can be reached, representing a non-productive complex $\overline{C(AB)}$, here placed on the left of the diagram. **B** Limiting barrier as a function of the substrate concentration $[A]$ and the interaction strength ϵ^-_{AA}, for $\epsilon^+_{AB} = 10$, and no product, $[AB] = 0$. The red line represents the optimal interaction strength with three different regimes, (a), (b), (c), depending on which two barriers are in trade-off (see Supplementary Material).

In summary, catalysis of the reaction $A + B \to AB$ is favored by a large reaction barrier ϵ^+_{AB}, a large reaction volume L^2 and a particular, finite value of the interaction strength ϵ^-_{AA} that depends on ϵ^+_{AB} and L^2.

Optimal cycling time in the absence of products. Having determined the conditions under which a molecule C acts as a catalyst, we now analyze how the catalytic turnover depends on the concentration of substrates $[A] = [B]$. To this end, we can ignore the spontaneous reaction. As a first step, we also assume that products are systematically removed so that $[AB] = 0$. The rates of the elementary processes along the cycle are formally obtained by replacing L^{-2} by $[A]$ in Eq. (2), to account for the possible presence of multiple substrates. In other terms, in what follows, we approximate the constant diffusion rates to 1 so that the reaction rates simply become proportional to the concentration of the species. The Markov chain for the complete cycle can be represented graphically as a kinetic energy diagram[62] (Fig. 3A).

Kinetic barrier diagrams provide a rigorous framework for systematically analyzing different growth regimes, defined by different limiting processes. For our model, each of the five states i in the diagram ($i = 1$ for C, $i = 2$ for CA, $i = 3$ for $C(A + B)$, $i = 4$ for $C(AB)$ and $i = 5$ for $C + AB$) is represented at an energy level G_i and successive states are separated by transition states at energy level $G_i^\ddagger$, such that the differences of energies between states and transition states report the rates as

$$k_i = e^{-(G_i^\ddagger - G_i)}, \quad k_{-i} = e^{-(G_i^\ddagger - G_{i+1})}. \tag{3}$$

In this representation, the mean cycling time has a simple expression[62–64],

$$T^0_{\text{cycle}}([A]) = \sum_{1 \le i \le j \le 4} e^{G_j^\ddagger - G_i} \tag{4}$$

where the sum is over each pair $i \le j$ of transition state j following a ground state i and where the superscript "0" indicates that no product is present. This sum is typically dominated by its largest term so that

$$T^0_{\text{cycle}}([A]) \approx e^{\max_{1 \le i \le j \le 4}(G_j^\ddagger - G_i)}. \tag{5}$$

The exponent defines the limiting barrier, also known as the energy span[63,65], which is represented in kinetic barrier diagrams by the largest difference of energy between successive—but not necessarily consecutive—levels. This limiting barrier formalizes the intuitive but problematic notion of "limiting step", which takes only into account successive levels[65]. As we show below, reducing the estimation of the mean cycling time to the determination of the limiting barrier simplifies the analysis and the interpretation of the results without qualitatively changing the conclusions.

Limiting barriers can be of two types, direct barriers between successive states and indirect barriers between non-successive states. Direct barriers report the mean time to perform one elementary transition. The dependence of the direct barriers $G_i^\ddagger - G_i = -\ln k_i$ on the parameters is given by Eq. (2),

$$\begin{aligned} G_1^\ddagger - G_1 &\approx -\ln[A] - \ln 2, \\ G_2^\ddagger - G_2 &\approx -\ln[A], \\ G_3^\ddagger - G_3 &\approx \epsilon^+_{AB}, \\ G_4^\ddagger - G_4 &\approx 2\epsilon^-_{AA}. \end{aligned} \tag{6}$$

The first two barriers describe the diffusion of substrates to the catalyst, the third barrier is the dimerization reaction on the catalyst, and the last the release of the product.

The total cycling time is, however, more than the addition of these elementary transition times. Indeed, once a state has been reached, the next elementary transition may be a backward transition and not a forward one, corresponding to a recrossing event. This is the origin of the indirect barriers between non-consecutive states, given by

$$\begin{aligned} G_2^\ddagger - G_1 &= \ln \tfrac{k_{-1}}{k_1 k_2} \approx -\epsilon^-_{AA} - 2\ln[A] - \ln 2, \\ G_3^\ddagger - G_1 &= \ln \tfrac{k_{-1}k_{-2}}{k_1 k_2 k_3} \approx -2\epsilon^-_{AA} + \epsilon^+_{AB} - 2\ln[A], \\ G_3^\ddagger - G_2 &= \ln \tfrac{k_{-2}}{k_2 k_3} \approx -\epsilon^-_{AA} + \epsilon^+_{AB} - \ln[A] + \ln 2. \end{aligned} \tag{7}$$

These indirect barriers are all smaller than the backward direct barriers are higher. Hence, a short cycling time requires not only low forward direct barriers but also high backward direct barriers. As apparent in Eqs. (6) and Eqs. (7), the different barriers are not independent but controlled by the same physical and chemical parameters. These relationships capture the essential trade-offs involved in the design of catalysis.

For instance, at low substrate concentration, the optimal interaction energy is $\hat{\epsilon}^-_{AA} = (\epsilon^+_{AB} - 2\ln[A])/4$. Consistent with the Sabatier principle, this optimum strikes a balance between the indirect barrier for

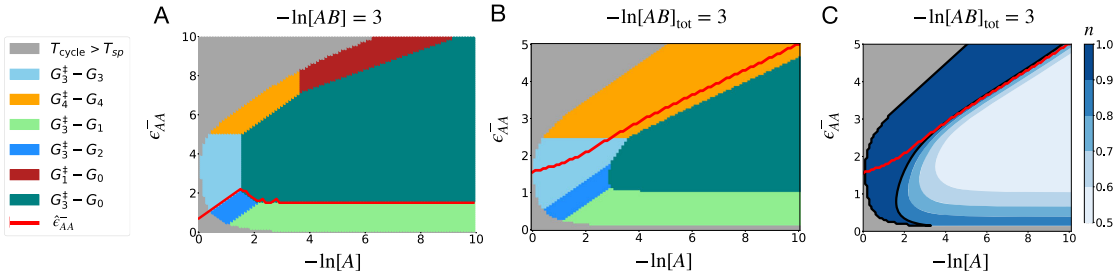

Fig. 4 | Limiting barriers in the presence of products. A Limiting barriers for a given concentration of free product $[AB]$. Compared to Fig. 3B, the limiting barrier can be associated with product inhibition (regimes in darker colors), in which case $T_{cycle} \approx T_{inhib}$. As a consequence, the optimal interaction strength ϵ_{AA}^- is changed (red line). **B** Limiting barriers when fixing the total concentration of autocatalyst $[AB]_{tot}$ instead of the concentration of free autocatalyst $[AB]$. The results are similar at low ϵ_{AA}^-, when $[AB]_{tot} \simeq [AB]$, but different at large ϵ_{AA}^-, when $[AB]_{tot} \simeq [(AB)(AB)]$. In these two cases, $[\overline{(AB)(AB)}] \ll [AB]_{tot}$, implying two opposite limits with no product inhibition and, therefore, exponential growth. **C** Reaction order n, as computed from simulations of the ordinary differential equations describing the Markov model (see Methods). In comparison to B, we see that $n < 1$ even in regions where the limiting barrier is not associated with product inhibition. This is because product inhibition is always present, even when it does not control the limiting barrier. A value $n > 0.9$ is nevertheless observed for a large range of parameter values (dark blue).

substrate binding and dimerization $G_3^\ddagger - G_1$ (in green in Fig. 3B), which is diminished by increasing ϵ_{AA}^-, and the direct barrier for product release $G_4^\ddagger - G_4$ (in orange in Fig. 3B), which is conversely increased by increasing ϵ_{AA}^-. The same reasoning applies at higher substrate concentrations, where the direct barrier for product release is in trade-off with other indirect barriers related to substrate binding (segments (a) and (b) in Fig. 3B, see Supplementary Material).

The analysis of limiting barriers in kinetic barrier diagrams thus reveals how different trade-offs control the design of optimal catalysts, depending on chemical and physical parameters (Fig. 3B).

Optimal cycling time in the presence of products. We now extend the analysis to the presence of free products, $[AB] \neq 0$. The presence of a product generally increases the mean cycling time, because a catalyst can bind to a product instead of a substrate, thus forming a non-productive complex that we denote $\overline{C(AB)}$. This non-productive complex $\overline{C(AB)}$ is physically indistinguishable from the unreleased complex $C(AB)$ that constitutes the last step along a catalytic cycle (Fig. 1A) but the recognition that they are two different kinetic states is key to our analysis. Since $\overline{C(AB)}$ is a complex with a previously free AB, while $C(AB)$ is a complex with a newly made AB, they are indeed associated with two distinct constraints on catalysis, namely product inhibition and product release. Formally, Eq. (1) already accounts for product release, and additionally accounting for product inhibition is done by extending it to include

$$\overline{C(AB)} \underset{k_{-I}}{\overset{k_I}{\rightleftharpoons}} C + AB \tag{8}$$

where $k_I \approx k_{-4} \approx [AB]$ and $k_{-I} \approx e^{-2\epsilon_{AA}^-}$.

The total mean cycling time $T_{cycle}([A], [AB])$ is then increased by the mean time $T_{inhib}([A], [AB])$ spent in the inhibited state $\overline{C(AB)}$,

$$T_{cycle}([A], [AB]) = T^0_{cycle}([A]) + T_{inhib}([A], [AB]). \tag{9}$$

The slowdown due to product inhibition is a particular form of competitive inhibition where the product itself acts as the inhibitor[66].

$T_{inhib}([A], [AB])$ can be expressed by extending the kinetic barrier diagram to include a state $i = 0$ associated with $\overline{C(AB)}$, leading to

$$T_{inhib}([A], [AB]) = \sum_{i=1}^{3} e^{G_i^\ddagger - G_0}, \tag{10}$$

where the new kinetic barriers to consider are obtained from the previous ones as

$$G_i^\ddagger - G_0 = G_i^\ddagger - G_1 + \ln \frac{k_I}{k_{-I}} \tag{11}$$

for $i = 1, 2, 3$, leading to

$$\begin{aligned} G_1^\ddagger - G_0 &\approx 2\epsilon_{AA}^- - \ln[A] + \ln[AB] - \ln 2, \\ G_2^\ddagger - G_0 &\approx \epsilon_{AA}^- - 2\ln[A] + \ln[AB] - \ln 2, \\ G_3^\ddagger - G_0 &\approx \epsilon_{AB}^+ - 2\ln[A] + \ln[AB]. \end{aligned} \tag{12}$$

As shown in Fig. 4A, those additional barriers can dominate the others, leading the mean cycling time to be limited by product inhibition, $T_{cycle} \approx T_{inhib}$. In particular, this happens for large relative concentration of products, $[AB] \gg [A]$, such that the catalyst is more likely to bind a product than a substrate, and for large interaction strength with respect to the concentration of product, $\epsilon_{AA}^- \gg -\ln[AB]/2$, such that the time spent in the inhibited complex $\overline{C(AB)}$ is long (Supplementary Material). Since the barriers associated with product inhibition increase with ϵ_{AA}^-, one consequence of the accumulation of products is generally a decreased optimal interaction strength, as illustrated in Fig. 4A.

Growth laws for minimal autocatalysts

Production rate. Assuming a buffered concentration of free substrates A and B, and a negligible spontaneous reaction, the rate of product formation is obtained from the mean cycling time as[67]

$$\frac{d[AB]_{tot}}{dt} = \frac{1}{T_{cycle}([A], [AB])}[C]_{tot}, \tag{13}$$

where $[AB]_{tot}$ is the total concentration of products, including those which, after being formed, bind to a catalyst or a substrate, and where $[C]_{tot}$ is the total concentration of catalysts, either free or bound. With standard catalysis, $[C]_{tot}$ remains constant and the rate of product formation is simply proportional to it. With autocatalysis, however, $C = AB$, and the total concentration of catalysts increases as more products are formed. Eq. (13) becomes

$$\frac{d[AB]_{tot}}{dt} = \frac{1}{T_{cycle}([A], [AB])}[AB]_{tot}, \tag{14}$$

which is generally a non-linear function of $[AB]_{tot}$ since $[AB]$ is itself a function of $[AB]_{tot}$. Special conditions are therefore required for exponential

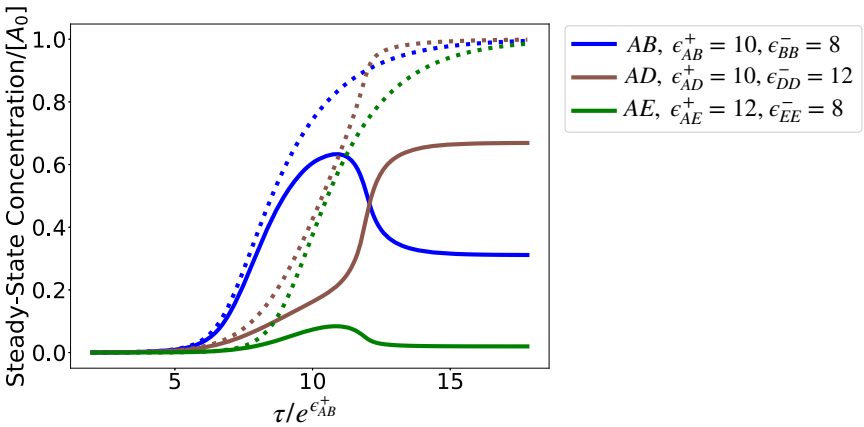

Fig. 5 | Competition for a common limiting resource. Steady-state concentrations of non-competing (dotted lines) and competing (plain lines) autocatalysts *AB*, *AD*, and *AE* in a chemostat, as a function of the residence time τ. The steady-state concentrations are normalized by the concentration at which the substrates are supplied, $[A]_0 = [B]_0 = [C]_0 = [D]_0 = e^{-10}$. While low residence times favor *AB*, higher residence times favor autocatalysts *AD*. The figure also illustrates how an autocatalyst of lower efficiency, here *AE*, can be excluded.

growth to occur, where $d[AB]_{tot}/dt = k[AB]_{tot}$ with a rate k independent of $[AB]_{tot}$.

Conditions for exponential growth. The decomposition of the cycling time in Eq. (9) makes explicit the conditions for exponential growth to occur: since $T_{inhib}([A], [AB])$ depends on $[AB]$ but $T^0_{cycle}([A])$ does not, we must have $T^0_{cycle}([A]) \gg T_{inhib}([A], [AB])$, i.e., product inhibition must be negligible.

Figure 4A shows that this occurs when release rates significantly exceed diffusion rates, $\epsilon^-_{AA} \ll -\ln[A]$, which a systematic analysis of limiting barriers confirms (Supplementary Material). Figure 4A is drawn for a fixed concentration of free product $[AB]$, but it is often more informative to fix the total concentration of products, $[AB]_{tot}$, which better reflects the progression of the dynamics and the consumption of resources—a determining factor when considering competitions as below.

When considering a fixed $[AB]_{tot}$, Fig. 4B also shows that product inhibition is negligible when $\epsilon^-_{AA} \ll -\ln[A]$. This coincides with the results of Fig. 4A because in this case most products are free, i.e., $[AB]_{tot} \approx [AB]$, which implies that inhibiting complexes $\overline{(AB)(AB)}$ are negligible (Fig. S6). However, a significant difference appears in the opposite limit $\epsilon^-_{AA} \gg -\ln[A]$ where, in contrast to Fig. 4A, B shows an extended regime where product inhibition is negligible (in orange). In this regime, most products are in the form of unreleased complexes $(AB)(AB)$ and therefore also not form inhibiting complexes $\overline{(AB)(AB)}$ (Fig. S6). The distinction made in Eq. (8) and Fig. 3A between the physically identical but kinetically distinct states of unreleased and inhibiting complexes is critical to understanding this regime. Indeed, without this distinction, the total concentration of duplexes, $[(AB)(AB)] + [\overline{(AB)(AB)}]$, would simply appear to increase with higher interaction strength, masking the underlying shift from faster product release and higher product inhibition—high $[\overline{(AB)(AB)}]$—to slower product release but lower product inhibition—high $[(AB)(AB)]$.

Reducing the analysis to the identification of limiting barriers is an approximation that provides necessary but not sufficient conditions for strictly exponential autocatalysis: a barrier associated with product inhibition may indeed contribute significantly to the cycling time even if it is not the limiting barrier. To go beyond this approximation, we approximate the dynamics with the phenomenological equation $d[AB]_{tot}/dt = k[AB]^n_{tot}$ (see Methods) and analyze the conditions under which $n \approx 1$. We verify that these conditions are more demanding than those for which the limiting barrier is not associated with product inhibition, but nevertheless observe that autocatalytic growth is nearly exponential growth for a large number of parameters, even taking into account the constraint that the growth rate must exceed the spontaneous reaction rate (Fig. 4C).

The conditions for exponential growth, either weak or large interaction strengths, are in direct contrast to the conditions for minimal cycling time which, following the Sabatier principle, requires an intermediate interaction strength (Fig. 2B). As illustrated in Fig. 4C, this translates into a generic trade-off between the reaction constant k and the reaction order n. The strength of this trade-off depends, however, on the values of the interaction barrier ϵ^+_{AB}: increasing ϵ^+_{AB} mitigates this trade-off, drawing the optimal values of k and n closer together (Fig. S7). This occurs for large values of both ϵ^+_{AB} and ϵ^-_{AA}, when $\epsilon^+_{AB} > \epsilon^-_{AA} > -\ln[AB]/2$. Indeed, as ϵ^+_{AB} increases, the optimal ϵ^-_{AA} also increases according to Sabatier's principle, until a point where it saturates and where no free autocatalyst remains, thereby preventing product inhibition.

Competition rules for minimal autocatalysts

One consequence of product inhibition is that the cycling time alone does not determine the outcome of competitions between autocatalysts. To demonstrate this, we consider in Fig. 5 a simple setting with three autocatalysts in a chemostat, *AB*, *AD*, and *AE*, all competing for a common resource *A*. Substrates *A*, *B*, *D*, and *E* are supplied at a uniform constant rate τ^{-1}, and all molecules are diluted at the same rate τ^{-1}, so that τ represents the typical residence time in the chemostat.

Previous theoretical investigations have emphasized a fundamental difference between exponential ($n = 1$) and sub-exponential ($n < 1$) autocatalysts in such conditions: while exponential autocatalysts invariably compete to exclude one another, sub-exponential autocatalysts typically coexist[6–8,68]. In recent work, we considered the competition of autocatalysts of different order n and noted that, somewhat counterintuitively, a sub-exponential autocatalyst ($n < 1$) can exclude an exponential one ($n = 1$) if its reaction constant k is sufficiently large[69]. This occurs, notably, at high dilution rates, when the mean residence time of the molecules in the chemostat is short relative to the mean cycling time, or, equivalently, when resources are scarce. In such conditions, autocatalysts are kept at a low concentration, mitigating product inhibition and making reaction constants k the determining factor. This is verified in this model, where in comparison to our previous work, the phenomenological parameters k and n are constrained by the physical parameters of the autocatalysts and by extrinsic conditions. When competing *AB* with *AD*, an autocatalyst of higher n but lower k, *AD* dominates *AB* only for sufficiently large values of τ (Fig. 5A). Thus, not only does an optimal cycling rate not guarantee dominance, but no intrinsic property of the autocatalyst guarantees it independently of the extrinsic conditions in which the competition takes place. Finally, this figure also illustrates how multiple autocatalysts competing for the same

resource may either coexist or exclude each other, despite no strict exponential growth (n is never strictly 1).

Discussion

Our analysis of minimal autocatalysis reveals that contrary to what previous empirical attempts might have suggested, exponential autocatalysts can be designed without recourse to complex internal mechanisms, complicated geometries, or external drives. In particular, since von Kiedrowski's original study[19], past limitations are well-known to originate from product inhibition, the propensity of autocatalysts to bind to each other after they have been produced. Our analysis concurs with von Kiedrowski's in recognizing product inhibition as a fundamental limitation of autocatalytic growth, which can, however, be circumvented by an appropriate choice of physical and chemical parameters.

Von Kiedrowski's study hinged on two assumptions: the chemical step is the limiting step of the cycle, and the substrate concentration is much higher than that of the autocatalyst[19]. These assumptions permit the definition of an autocatalytic cycle with just three parameters: K_1, the equilibrium association constant between substrates and templates, K_2, the equilibrium association constant between templates, and ϵ^+_{AB}, the dimerization barrier—with our notations, $K_1 = k_1k_2/(k_{-1}k_{-2})$ and $K_2 = k_{-4}/k_4 = k_I/k_{-I}$. From these three parameters and the concentration of the various molecular species, the reaction order n can be determined [see Eq. (S4)]. By expressing K_1 and K_2 as a function of temperature, Von Kiedrowski found that exponential growth is possible at low and high temperatures, regimes he called "weak" and "strong" exponential growth respectively. However, the assumptions required to obtain this result are rather restrictive in practice. In particular, they may not be valid for exponential autocatalysts, which are generally limited by product release, or when studying their competition for a common resource, when the substrate is less abundant than the autocatalyst.

Our approach, based on analyzing limiting barriers, enables us to explore autocatalytic growth beyond these assumptions. We thus recover Kiedrowski's two exponential growth regimes: weak and strong exponential growths are respectively associated with the phases limited by $G_3^\ddagger - G_1$ and $G_4^\ddagger - G_4$ in Fig. 4B (see also Figs. S6–S8). We find, however, that these phases extend beyond the range of parameters to which Kiedrowski's analysis was limited. The weak exponential growth regime is of limited interest as the exponential growth is then slower than the spontaneous reaction (Fig. 4C). The strong exponential regime, on the other hand, can dominate the spontaneous reaction for a much wider range of parameters than Kiedrowski's assumptions allow. Furthermore, our study elucidates how constraints related to product inhibition differ from those due to product release, affecting reaction rate but not necessarily altering reaction order.

The focus on exponential growth stems from the exclusion principle that it implies, which is often considered as a core principle of natural selection[7,19]: two exponential autocatalysts cannot coexist if they depend on the same resource. Our results underline that exponentiality is not an intrinsic property of an autocatalyst, but crucially depends on extrinsic conditions, and that exclusion can occur in the absence of exponential growth. However, it can also be argued that the absence of strict exclusion is in itself conducive to the emergence of diversity and of evolution by natural selection[4,6].

The key feature of our model is its definition based solely on physical principles: all possible molecules and reactions are derived from interaction potentials between elementary "atoms". This reveals how different rate constants are in trade-off because they depend on the same physical parameters. Our analysis of simple competitions between autocatalysts can thus go beyond previous studies where product inhibition is phenomenologically described by a reaction constant k and a reaction order n[6,7,68]. In particular, our model demonstrates how n and k can be in a trade-off: maximizing n to achieve exponential growth ($n = 1$) typically comes at the expense of a low k. In competitions between autocatalysts, whether a large k or a large n is advantageous depends on the chemical environment. If resources are abundant, autocatalysts with higher reaction order tend to prevail, but, if resources are scarce, autocatalysts with higher reaction constants have an advantage, irrespective of their reaction order. An exclusive focus on the reaction order n may therefore be misleading.

We defined a generic and simple model with a view to its implementation in various molecular or colloidal systems. First, we chose the catalytic mechanism to be of the most basic form: the (auto)catalyst catalyzes a dimerization reaction simply by increasing the frequency of interaction between substrates when they are attached to it. This form of catalysis by proximity is universal and applies irrespective of whether the dimerization barrier is entropic or enthalpic. The parameters in our model also have their direct counterpart in almost all chemical contexts. For example, in the realm of nucleic acids, inter-dimer interactions correspond to base pairing via hydrogen bonds, while stronger intra-dimer interactions with an association barrier correspond to nearly irreversible endothermic phosphodiester covalent bonds[70,71]. In the realm of colloids whose interactions are mediated by the hybridization of complementary DNA strands or by magnetic forces, association barriers can correspond to electrostatic repulsion, to an entropic barrier due to steric effects, or to linkage-mediated interactions[28,72–78]. In this context, interaction strengths are typically of the order of a few k_BT, and unbinding occurs within <1 min[59,79]. In this case, exponential growth would require interaction strengths of the order of 10 k_BT, depending on the relative concentration of substrate over the product (Fig. S8). Exponential autocatalysts would then replicate within hours, in the range of experimentally accessible timescales.

For the sake of simplicity, we assumed that no molecule larger than four in size can form. For example, polymeric chains $ABABA\ldots$ where a B interacts with two A simultaneously are excluded. This is straightforwardly the case with molecular systems that are intrinsically anisotropic[9,18,77] but, may be more difficult to impose on isotropic colloids[72]. However, a simple extension of the model translates this assumption into a constraint on the valence of atoms that is easier to implement. Our analysis indeed applies without change to the cross-catalysis of two dimers AB and $A'B'$, where each type of atom is constrained to interact with at most two atoms of two different types, A with B and A', B with A and B', A' with A and B', B' with A' and B'. DNA or RNA replication works by such cross-catalysis between complementary strands[18,20,25]. With spherical colloids, cross-catalysis can for instance be implemented by limiting interactions to patches[77] (Fig. S4). However, we constrained the size of the molecules only to simplify the analysis, and the possibility of forming larger molecules is obviously of interest on its own.

The trade-offs that constrain our model fundamentally stem from its deliberate simplicity. In particular, the tension between chemical acceleration, on the one hand, and product release and inhibition, on the other, which underlies the Sabatier principle and plays a key role in our analysis, can be overcome by a variety of mechanisms[61,80]. In all practical cases, however, these mechanisms involve large and complex molecules. Our analysis shows that they are not prerequisites for exponential growth or selection by exclusion. This resolves an apparent paradox in origin-of-life scenarios that seek to explain complexity as a consequence of Darwinian evolution, but require complex mechanisms for such evolution to take place.

Methods

Molecular dynamics simulations

Brownian molecular dynamics (MD) simulations were carried out in HoomD 3.5.0[81], using a time step $\Delta t = 10^{-5}$, periodic boundary conditions, and a damping constant $\gamma = 10$, corresponding to a translational diffusion coefficient $k_BT/\gamma = 0.1$ length^2/time, comparable to values measured in experiments with colloids[76]. The potential between two particles X and Y is

taken to be

$$U_{XY}(r) = \begin{cases} \epsilon^{-}_{XY} u(r) + \epsilon^{+}_{XY} & \text{if } r \le r_{c,} \\ -\epsilon^{-}_{XY} u\left(r - r_c + r_{\min}\right) & \text{if } r_c \le r \le 2r_c - r_{\min} \end{cases}$$

where ϵ^{-}_{XY} and ϵ^{+}_{XY} represent the activation barriers for dissociation and association, respectively. The potential $u(r)$ is a generalization of the Wang-Frenkel potential[58], with a cutoff value of $r_c = 1.1$,

$$u(r) = \begin{cases} \alpha(r_c)\left[\left(\frac{\sigma}{r}\right)^2 - 1\right]\left[\left(\frac{r_c}{r}\right)^2 - 1\right]^2 & \text{for } r \le r_c \\ 0 & \text{for } r > r_c. \end{cases}$$

Markov model

We approximate catalytic cycles by Markov chains. With two atoms A and B, the Markov chain involves a total of 15 transitions. First, the spontaneous reaction $A + B \to AB$, with rate $[A][B]e^{-\epsilon^{+}_{AB}}$. Second, 7 association reactions, $AB + A \to AAB$, $AB + B \to ABB$, $AAB + B \to AABB$, $ABB + A \to AABB$, $AB + AB \to \overline{ABAB}$, $A + A \to AA$ and $B + B \to BB$, with rates proportional to the reactant concentrations. Third, the dimerization reaction on the autocatalyst, $AABB \to ABAB$, with rate $[AABB]e^{-\epsilon^{+}_{AB}}$. Finally, 8 dissociation reactions, $AA \to A + A$, $BB \to B + B$, $AAB \to A + AB$, $ABB \to B + AB$, $AABB \to B + AAB$, $AABB \to A + ABB$, with rates $e^{-\epsilon^{-}_{AA}}$, and $ABAB \to AB + AB$, $\overline{ABAB} \to AB + AB$ with rates $e^{-2\epsilon^{-}_{AA}}$. When considering two competing autocatalysts AB and AC sharing a common monomer, we ignore for simplicity the complexes that they may form, of the type $(AB)(AC)$, which are less stable than homotetramers $(AB)(AB)$.

We determine the steady state of the Markov chain by integrating numerically the ordinary differential equations that describe its dynamical evolution. We consider either a system with a fixed concentration of substrate [A]=[B], and other molecules accumulating (Fig. 4C), or in a chemostat (Fig. 5). In this later case, differential equations include the description of the introduction of substrates, $\emptyset \to A$ and $\emptyset \to B$, with rate $[A]_0/\tau$, and the dilution of all species, $X \to \emptyset$, with rate $1/\tau$.

Reaction order and reaction constant

We estimate a reaction order n and a reaction constant k such that $d[AB]_{\text{tot}}/dt = k[AB]^n_{\text{tot}}$ approximatively holds by integrating numerically the dynamical equations of the Markov chain with constant values of $[A] = [B]$, starting with $[AB] = 0$ and ending when reaching the targeted value of $[AB]_{\text{tot}}$. The values of k and n are then obtained by linear regression of $\ln(d[AB]_{\text{tot}}/dt)$ against $\ln([AB]_{\text{tot}})$.

Data availability

The datasets used to generate the figures in this study are available in the GitHub repository: https://github.com/YannS-source/Design_Autocatalysts.

Code availability

The molecular dynamics simulations were performed using the HoomD-Blue package 3.5. 0[81]. The specific code for our simulations is available in the Github repository: https://github.com/YannS-source/Design_Autocatalysts.

Received: 14 April 2024; Accepted: 23 July 2024;
Published online: 21 October 2024

References

1. Orgel, L. E. Molecular replication. *Nature* **358**, 203–209 (1992).
2. Eigen, M. & Winkler-Oswatitsch, R. *Steps Towards Life: A Perspective On Evolution*. (Oxford University Press, 1996).
3. Luisi, P. L. *The Emergence of Life: From Chemical Origins to Synthetic Biology*. (Oxford University Press, 2006).
4. Zachar, I. & Szathmáry, E. A new replicator: a theoretical framework for analysing replication. *BMC Biol.* **8**, 21 (2010).
5. Hanopolskyi, A. I., Smaliak, V. A., Novichkov, A. I. & Semenov, S. N. Autocatalysis: kinetics, mechanisms and design. *ChemSystemsChem* **3**, e2000026 (2021).
6. Szathmáry, E. & Gladkih, I. Sub-exponential growth and coexistence of non-enzymatically replicating templates. *J. Theor. Biol.* **138**, 55–58 (1989).
7. Scheuring, I. & Szathmáry, E. Survival of replicators with parabolic growth tendency and exponential decay. *J. Theor. Biol.* **212**, 99–105 (2001).
8. von Kiedrowski, G. & Szathmáry, E. Selection versus coexistence of parabolic replicators spreading on surfaces. *Selection* **1**, 173–180 (2005).
9. von Kiedrowski, G. A self-replicating hexadeoxynucleotide. *Angew. Chem. Int. Ed. Engl.* **25**, 932–935 (1986).
10. Zielinski, W. S. & Orgel, L. E. Autocatalytic synthesis of a tetranucleotide analogue. *Nature* **327**, 346–347 (1987).
11. Tjivikua, T., Ballester, P. & Rebek, J. Self-replicating system. *J. Am. Chem. Soc.* **112**, 1249–1250 (1990).
12. Wang, B. & Sutherland, I. O. Self-replication in a Diels-Alder reaction. *Chem. Commun.* **16**, 1495–1496 (1997).
13. Lee, D. H., Granja, J. R., Martinez, J. A., Severin, K. & Ghadiri, M. R. A self-replicating peptide. *Nature* **382**, 525–528 (1996).
14. Issac, R. & Chmielewski, J. Approaching exponential growth with a self-replicating peptide. *J. Am. Chem. Soc.* **124**, 6808–6809 (2002).
15. Kamioka, S., Ajami, D. & Rebek, J. Autocatalysis and organocatalysis with synthetic structures. *Proc. Natl. Acad. Sci. USA* **107**, 541–544 (2010).
16. Colomb-Delsuc, M., Mattia, E., Sadownik, J. W. & Otto, S. Exponential self-replication enabled through a fibre elongation/breakage mechanism. *Nat. Commun.* **6**, 7427 (2015).
17. Kosikova, T. & Philp, D. Two synthetic replicators compete to process a dynamic reagent pool. *J. Am. Chem. Soc.* **141**, 3059–3072 (2019).
18. Zhuo, R. et al. Litters of self-replicating origami cross-tiles. *Proc. Natl. Acad. Sci. USA* **116**, 1952–1957 (2019).
19. von Kiedrowski, G. in *Bioorganic Chemistry Frontiers* (eds Dugas, H. & Schmidtchen, F. P.) Vol. 3, 113–146. (Springer, 1993).
20. Sievers, D. & von Kiedrowski, G. Self-replication of hexadeoxynucleotide analogues: autocatalysis versus cross-catalysis. *Chem. Eur. J.* **4**, 629–641 (1998).
21. Szathmáry, E. & Maynard Smith, J. From replicators to reproducers: the first major transitions leading to life. *J. Theor. Biol.* **187**, 444–460 (1997).
22. Braun, D. PCR by thermal convection. *Mod. Phys. Lett. B* **18**, 775–784 (2004).
23. Wang, T. et al. Self-replication of information-bearing nanoscale patterns. *Nature* **478**, 225–228 (2011).
24. Carnall, J. M. A. et al. Mechanosensitive self-replication driven by self-organization. *Science* **327**, 1502–1506 (2010).
25. Zhang, D. Y., Turberfield, A. J., Yurke, B. & Winfree, E. Engineering entropy-driven reactions and networks catalyzed by DNA. *Science* **318**, 1121–1125 (2007).
26. Zhang, R., Walker, D. A., Grzybowski, B. A. & Olvera de la Cruz, M. Accelerated self-replication under non-equilibrium, periodic energy delivery. *Angew. Chem. Int. Ed.* **53**, 173–177 (2014).
27. Fernando, C., von Kiedrowski, G. & Szathmáry, E. A stochastic model of nonenzymatic nucleic acid replication: "Elongators" sequester replicators. *J. Mol. Evol.* **64**, 572–585 (2007).
28. Dempster, J. M., Zhang, R. & Olvera De La Cruz, M. Self-replication with magnetic dipolar colloids. *Phys. Rev. E* **92**, 042305 (2015).
29. Penrose, L. S. & Penrose, R. A self-reproducing analogue. *Nature* **179**, 1183–1183 (1957).
30. Penrose, L. S. Mechanics of self-reproduction. *Ann. Hum. Genet.* **23**, 59–72 (1958).
31. Penrose, L. S. Self-reproducing machines. *Sci. Am.* **200**, 105–117 (1959).
32. Virgo, N., Fernando, C., Bigge, B. & Husbands, P. Evolvable physical self-replicators. *Artif. Life* **18**, 129–142 (2012).

33. Abe, H. & Kool, E. T. Destabilizing universal linkers for signal amplification in self-ligating probes for RNA. *J. Am. Chem. Soc.* **126**, 13980–13986 (2004).
34. Osuna Gálvez, A. & Bode, J. W. Traceless templated amide-forming ligations. *J. Am. Chem. Soc.* **141**, 8721–8726 (2019).
35. Cabello-Garcia, J., Bae, W., Stan, G. B. V. & Ouldridge, T. E. Handhold-mediated strand displacement: a nucleic acid based mechanism for generating far-from-equilibrium assemblies through templated reactions. *ACS Nano* **15**, 3272–3283 (2021).
36. Juritz, J., Poulton, J. M. & Ouldridge, T. E. Minimal mechanism for cyclic templating of length-controlled copolymers under isothermal conditions. *J. Chem. Phys.* **156**, 074103 (2022).
37. Michaelis, J., Roloff, A. & Seitz, O. Amplification by nucleic acid-templated reactions. *Org. Biomol. Chem.* **12**, 2821–2833 (2014).
38. Kim, D.-E. & Joyce, G. F. Cross-catalytic replication of an RNA ligase ribozyme. *Chem. Biol.* **11**, 1505–1512 (2004).
39. Lincoln, T. A. & Joyce, G. F. Self-sustained replication of an RNA enzyme. *Science* **323**, 1229–1232 (2009).
40. Zeravcic, Z. & Brenner, M. P. Self-replicating colloidal clusters. *Proc. Natl. Acad. Sci. USA* **111**, 1748–1753 (2014).
41. Semenov, S. N. et al. Autocatalytic, bistable, oscillatory networks of biologically relevant organic reactions. *Nature* **537**, 656–660 (2016).
42. Cafferty, B. J. et al. Robustness, entrainment, and hybridization in dissipative molecular networks, and the origin of life. *J. Am. Chem. Soc.* **141**, 8289–8295 (2019).
43. Blokhuis, A., Lacoste, D. & Nghe, P. Universal motifs and the diversity of autocatalytic systems. *Proc. Natl. Acad. Sci. USA* **117**, 25230–25236 (2020).
44. Ameta, S. et al. Darwinian properties and their trade-offs in autocatalytic RNA reaction networks. *Nat. Commun.* **12**, 842 (2021).
45. Kauffman, S. A. Cellular homeostasis, epigenesis and replication in randomly aggregated macromolecular systems. *J. Cybern.* **1**, 71–96 (1971).
46. Eigen, M. & Schuster, P. A principle of natural self-organization. *Naturwissenschaften* **64**, 541–565 (1977).
47. Szostak, J. W. An optimal degree of physical and chemical heterogeneity for the origin of life? *Philos. Trans. R. Soc. B Biol. Sci.* **366**, 2894–2901 (2011).
48. Liu, Y. & Sumpter, D. J. T. Mathematical modeling reveals spontaneous emergence of self-replication in chemical reaction systems. *J. Biol. Chem.* **293**, 18854–18863 (2018).
49. Hordijk, W. A history of autocatalytic sets. *Biol. Theory* **14**, 224–246 (2019).
50. Hordijk, W., Steel, M. & Kauffman, S. A. Molecular diversity required for the formation of autocatalytic sets. *Life* **9**, 23 (2019).
51. Hordijk, W., Shichor, S. & Ashkenasy, G. The influence of modularity, seeding, and product inhibition on peptide autocatalytic network dynamics. *ChemPhysChem* **19**, 2437–2444 (2018).
52. Eigen, M. Selforganization of matter and the evolution of biological macromolecules. *Naturwissenschaften* **58**, 465–523 (1971).
53. Matsumura, S. et al. Transient compartmentalization of RNA replicators prevents extinction due to parasites. *Science* **354**, 1293–1296 (2016).
54. Rivoire, O. A role for conformational changes in enzyme catalysis. *Biophys. J.* **123**, 1–16 (2024).
55. Muñoz-Basagoiti, M., Rivoire, O. & Zeravcic, Z. Computational design of a minimal catalyst using colloidal particles with programmable interactions. *Soft Matter* **19**, 3933–3939 (2023).
56. Sakref, Y., Muñoz-Basagoiti, M., Zeravcic, Z. & Rivoire, O. On kinetic constraints that catalysis imposes on elementary processes. *J. Phys. Chem. B* **127**, 10950–10959 (2023).
57. Rogers, W. B., Shih, W. M. & Manoharan, V. N. Using DNA to program the self-assembly of colloidal nanoparticles and microparticles. *Nat. Rev. Mater.* **1**, 1–14 (2016).
58. Wang, X., Ramírez-Hinestrosa, S., Dobnikar, J. & Frenkel, D. The Lennard-Jones potential: when (not) to use it. *Phys. Chem. Chem. Phys.* **22**, 10624–10633 (2020).
59. Cui, F., Marbach, S., Zheng, J. A., Holmes-Cerfon, M. & Pine, D. J. Comprehensive view of microscopic interactions between DNA-coated colloids. *Nat. Commun.* **13**, 2304 (2022).
60. Medford, A. J. et al. From the Sabatier principle to a predictive theory of transition-metal heterogeneous catalysis. *J. Catal.* **328**, 36–42 (2015).
61. Rivoire, O. How flexibility can enhance catalysis. *Phys. Rev. Lett.* **131**, 088401 (2023).
62. Penocchio, E. & Ragazzon, G. Kinetic barrier diagrams to visualize and engineer molecular nonequilibrium systems. *Small* **19**, 2206188 (2023).
63. Kozuch, S. & Martin, J. M. What makes for a bad catalytic cycle? A theoretical study on the suzuki-miyaura reaction within the energetic span model. *ACS Catal.* **1**, 246–253 (2011).
64. Park, C. Describing chemical kinetics in the time dimension with mean reaction time. *bioRxiv* https://doi.org/10.1101/2022.02.01.478700 (2022).
65. Kozuch, S. & Shaik, S. How to conceptualize catalytic cycles? The energetic span model. *Acc. Chem. Res.* **44**, 101–110 (2011).
66. Bezerra, R. M. F., Pinto, P. A., Fraga, I. & Dias, A. A. Enzyme inhibition studies by integrated Michaelis-Menten equation considering simultaneous presence of two inhibitors when one of them is a reaction product. *Comput. Methods Programs Biomed.* **125**, 2–7 (2016).
67. Ninio, J. Alternative to the steady-state method: derivation of reaction rates from first-passage times and pathway probabilities. *Proc. Natl. Acad. Sci. USA* **84**, 663–667 (1987).
68. Lifson, S. & Lifson, H. Coexistence and Darwinian selection among replicators: response to the preceding paper by Scheuring and Szathmary. *J. Theor. Biol.* **212**, 107–109 (2001).
69. Sakref, Y. & Rivoire, O. On the exclusion of exponential autocatalysts by sub-exponential autocatalysts. *J. Theor. Biol.* **579**, 111714 (2024).
70. Monnard, P.-A. Taming prebiotic chemistry: the role of heterogeneous and interfacial catalysis in the emergence of a prebiotic catalytic/information polymer system. *Life* **6**, 40 (2016).
71. Dickson, K. S., Burns, C. M. & Richardson, J. P. Determination of the free-energy change for repair of a DNA phosphodiester bond. *J. Biol. Chem.* **275**, 15828–15831 (2000).
72. Angioletti-Uberti, S., Varilly, P., Mognetti, B. M. & Frenkel, D. Mobile linkers on DNA-coated colloids: valency without patches. *Phys. Rev. Lett.* **113**, 128303 (2014).
73. Rogers, W. B. A mean-field model of linker-mediated colloidal interactions. *J. Chem. Phys.* **153**, 124901 (2020).
74. Wang, Y. et al. Colloids with valence and specific directional bonding. *Nature* **491**, 51–55 (2012).
75. Feng, L., Pontani, L.-L., Dreyfus, R., Chaikin, P. & Brujic, J. Specificity, flexibility and valence of DNA bonds guide emulsion architecture. *Soft Matter* **9**, 9816–9823 (2013).
76. Zhang, Y. et al. Multivalent, multiflavored droplets by design. *Proc. Natl. Acad. Sci. USA* **115**, 9086–9091 (2018).
77. Kress, R. N. & Jones, M. R. Colloidal interactions get patchy and directional. *Proc. Natl. Acad. Sci. USA* **117**, 15382–15384 (2020).
78. McMullen, A., Muñoz Basagoiti, M., Zeravcic, Z. & Brujic, J. Self-assembly of emulsion droplets through programmable folding. *Nature* **610**, 502–506 (2022).
79. Rogers, W. B., Sinno, T. & Crocker, J. C. Kinetics and non-exponential binding of DNA-coated colloids. *Soft Matter* **9**, 6412–6417 (2013).
80. Pérez-Ramírez, J. & López, N. Strategies to break linear scaling relationships. *Nat. Catal.* **2**, 971–976 (2019).
81. Anderson, J. A., Glaser, J. & Glotzer, S. C. HOOMD-blue: a Python package for high-performance molecular dynamics and hard particle Monte Carlo simulations. *Comput. Mater. Sci.* **173**, 109363 (2020).

Acknowledgements

We acknowledge funding from ANR-22-CE06-0037.

Author contributions

Y.S. and O.R. designed research, performed research, analyzed data, and wrote the paper.

Competing interests

The authors declare no competing interests.

Additional information

Supplementary information The online version contains supplementary material available at https://doi.org/10.1038/s42004-024-01250-y.

Correspondence and requests for materials should be addressed to Olivier Rivoire.

Peer review information *Communications Chemistry* thanks the anonymous reviewers for their contribution to the peer review of this work. A peer review file is available.